



JAAS

Measuring Signatures of Fuel Irradiation in Large Particle Samples

Journal:	<i>Journal of Analytical Atomic Spectrometry</i>
Manuscript ID	JA-ART-01-2021-000025.R1
Article Type:	Paper
Date Submitted by the Author:	17-Mar-2021
Complete List of Authors:	Hanson, Susan; Los Alamos National Laboratory, Nuclear and Radiochemistry Group Pollington, Anthony; Los Alamos National Laboratory, Nuclear and Radiochemistry Group

SCHOLARONE™
Manuscripts

Measuring Signatures of Fuel Irradiation in Large Particle Samples

Susan K. Hanson,* Anthony D. Pollington†

Understanding the operating history of a nuclear facility is one of the key goals in nuclear safeguards, enabling the verification of declared activities. This is accomplished via a number of mechanisms, including the analysis of samples collected at the facility. The best metrics for understanding and verifying the history of nuclear fuel are (1) actinide isotopic content and (2) actinide inter-element ratios. While techniques have long existed for measuring these values with high accuracy and precision in bulk samples, as samples become smaller – such as may be collected in environmental collection – new methods are required both for clean processing of pure samples, and for analysis of these small samples. This study describes a new extraction chromatography technique for recovering U, Pu, and Am from single small aliquots, and advanced mass spectrometry methods for high-precision and high-accuracy analysis of trace and ultra-trace levels of actinides. These techniques are applied to particle samples cut from fuel from a historic nuclear reactor. Ages calculated from Pu-Am chronometry of particles are in excellent agreement with the known operating history of the reactor.

Introduction

A principal goal of nuclear safeguards is to collect samples from nuclear facilities, and through the analysis of these samples, confirm that a declared history of facility operation is accurate.^{1–6}

For nuclear reactors, measurements of actinide elements in the nuclear fuel can provide information about the irradiation history.^{7–8} The concentrations of minor isotopes of uranium and plutonium, as well as the concentrations of other actinides, such as ²³⁶U, ²⁴⁰Pu, ²⁴¹Pu, ²⁴²Pu, Np, and Am, increases as the fuel is irradiated.⁹ Actinide inter-element ratios, such as the absolute ratio of uranium to plutonium in the nuclear fuel, can provide additional information about the final fuel composition after irradiation.¹⁰

The isotopic composition of nuclear fuel can change dramatically within different locations in the reactor. For many reactors, the degree of fuel burnup is known to vary along the axis of a fuel rod.^{11–13} In addition, radial effects have been documented, where the degree of burnup increases sharply near the outside edge of a fuel pellet.^{14–18} The radial effect is likely due to more effective neutron moderation in the small (100s of microns) local region near the fuel pellet edge.^{19–20} In order to understand this type of spatial effect in the reactor fuel, it is necessary to analyze small samples to provide adequate spatial resolution.

To this end, single particle analysis is an important tool for nuclear safeguards. Highly effective techniques for the *in situ* isotopic analysis of single particles have been developed, including secondary ionization mass spectrometry (SIMS), and laser ablation inductively coupled plasma mass spectrometry (LA-ICP-MS).^{21–24} Another effective method involves analyzing single particles by thermal ionization mass spectrometry (TIMS). In this technique, a particle is placed on the filament and analyzed as an individual sample, producing accurate uranium or plutonium isotopic ratios.^{25–28}

However, extracting actinide inter-element ratios from particle samples is a major challenge, and bulk isotopic analysis techniques can provide this additional information.²² Isotope dilution mass spectrometry (IDMS) involves addition of an

isotopic tracer to the sample, followed by equilibration and chemical purification, and finally measurement by mass spectrometry.^{29–30} Through isotope dilution, the different actinide constituents can be accurately quantified, allowing for highly accurate actinide inter-element ratios to be determined. The chemical purification of the sample ensures a high-quality result by removing interferences, like the polyatomic ion ²³⁸UH⁺ on ²³⁹Pu. In addition, chemical purification allows for separation of two different elements with very similar masses, such as ²⁴¹Pu and ²⁴¹Am, which cannot be resolved by current mass spectrometers. When both ²⁴¹Pu and ²⁴¹Am can be measured, information about the sample age and/or last chemical processing can be inferred through ²⁴¹Pu–²⁴¹Am chronometry.^{31–32}

This paper describes the development and application of optimized chemical purification and IDMS analysis methods for the analysis of single particles of nuclear fuel. The use of isotope dilution methods to analyze single particles is challenging due to the small quantities of the elements of interest, but provides substantial benefits in terms of accurate inter-element actinide ratios.^{23, 33–35} Purification of the samples chemically separates the elements of interest and provides resolution against isobars, allowing for separation and quantification of ²⁴¹Pu and ²⁴¹Am, as well as ²³⁸Pu and ²³⁸U.³⁶ These new techniques allow for the accurate measurement of U, Pu, and Am intra- and inter-element ratios in particle samples, and enable a clearer picture of fuel irradiation characteristics determined from the analysis of large nuclear fuel particles. The focus of this study is on the application of advanced chemical separations and high-precision isotopic analyses for the purpose of determining the operating conditions of nuclear reactors. However, the techniques developed here may also be applicable to studies of actinides in the environment, particularly where associated with colloids or particles and where accurate inter-element ratios provide a new facet of information.^{37–41}

Experimental

Belgian BR3 Fuel Samples

Samples from a spent fuel rod (I-334) from the Belgian (BR3) Pressurized Water Reactor (PWR) were prepared at the Hot Fuel Examination Facility (HFEF) at Idaho National Laboratory (INL). At INL, discs were cut from the BR3 fuel inside hot cells and then a central strip was cut from each disc. These strips were then

Nuclear and Radiochemistry Group, Los Alamos National Laboratory, Los Alamos, New Mexico, USA

* skhanson@lanl.gov

† pollington@lanl.gov

cast in epoxy mounts and removed from the HFEF to a dual focused ion beam/ scanning electron microscope (FIB/SEM).⁴²⁻
⁴³ Using the FIB, particles were cut from different axial locations along the length of the fuel rod. At each axial location, several different radial locations were sampled. Sample IDs and locations in the fuel rod are provided in Table 1. The particles were cubes of dimensions 10 x 10 x 10 μm or 20 x 20 x 20 μm .

Table 1 - Samples of Nuclear Fuel Obtained from INL

Sample ID	Sample dimensions (μm)	Axial sampling position	Axial distance from top of fuel rod (m)	Radial location (μm from edge)
1-A1	10 x 10 x 10	1	0.05	200
1-A2	10 x 10 x 10	1	0.05	200
1-B	10 x 10 x 10	1	0.05	400
1-C1	10 x 10 x 10	1	0.05	3000
1-C2	10 x 10 x 10	1	0.05	3000
1-C3	20 x 20 x 20	1	0.05	3000
1-C4	20 x 20 x 20	1	0.05	3000
2-A	10 x 10 x 10	2	0.22	5
2-B	10 x 10 x 10	2	0.22	40
2-C	10 x 10 x 10	2	0.22	1781
3-A	10 x 10 x 10	3	0.51	36
3-B	10 x 10 x 10	3	0.51	101
3-C	10 x 10 x 10	3	0.51	3755
4-A1	10 x 10 x 10	4	0.98	190
4-A2	10 x 10 x 10	4	0.98	190
4-B	10 x 10 x 10	4	0.98	900
4-C1	10 x 10 x 10	4	0.98	3003
4-C2	20 x 20 x 20	4	0.98	3173
4-C3	20 x 20 x 20	4	0.98	3173

Chemical Purification Methods

All chemical purifications were carried out in Savillex PFA labware that was cleaned with dilute (1 M) HNO_3 and rinsed three times with ultrapure 18.2 micro-ohm deionized water. All acids were Optima Grade purchased from Fisher Scientific, diluted as necessary with ultrapure deionized water, and stored in Nalgene Teflon bottles. All chemical processing was carried out in a chemical fume hood in a laboratory controlled for radioactive materials.

Each FIB sample was received mounted to a copper comb on an SEM stub enclosed in a vial (see Supporting Information). In the chemical fume hood, the SEM mount was removed from the vial and the copper comb with the FIB sample affixed was dissolved by submerging in 4 ml 8 M HNO_3 in a 15 ml Savillex PFA vial. One drop of concentrated HF was added, and the vial was heated to dryness at 140 $^\circ\text{C}$ overnight. The resulting residue was redissolved in 5 ml 3 M HNO_3 , forming a clear solution with no visible solid. A small fraction (ca. 1%) of this solution containing the dissolved sample was diluted by a factor of 40 with 2% v/v HNO_3 to estimate the actinide content using a Thermo X-Series quadrupole ICP-MS. Estimates of the total actinide concentrations obtained from the sample screening were used to determine appropriate tracer levels for the isotope dilution analysis.

Samples were traced with ^{233}U , ^{242}Pu or ^{244}Pu , and ^{243}Am and evaporated to dryness. The samples were purified using a sequential procedure for the separation of uranium, plutonium, and americium (Table 2). Several blank samples were prepared for analysis in parallel with the samples, including a dissolution blank, rinses of the vials that contained the original FIB samples, as well as several process blanks. The sequential purification was performed by extraction chromatography using a modified version of a previously published procedure.³⁴ The extraction chromatography column consisted of 0.5 ml of Eichrom UTEVA resin (100-150 μm) loaded into a 2 ml Biorad Biospin column. Full column details are provided in Table 2. The resin was cleaned by washing with 1 M HCl, and then conditioned with 3 M HNO_3 , followed by 7.2 M HNO_3 -0.3% H_2O_2 . The sample was dissolved in 7.2 M HNO_3 -0.3% H_2O_2 and loaded onto the column, with immediate collection of the Am fraction. The column was washed with additional 7.2 M HNO_3 -0.3% H_2O_2 , which was also collected as the Am fraction. The column was washed with 9 M HCl, followed by 5 M HCl-0.05 M oxalic acid, with collection of the Pu fraction during both steps. The uranium was eluted with 1 M HCl. The uranium fraction was evaporated to dryness, dissolved in 2% HNO_3 , and analyzed by multicollector (MC)-ICP-MS. Plutonium and americium fractions were further purified using established procedures,⁴⁴⁻⁴⁵ and the final purified fractions analyzed by MC-ICP-MS and alpha spectrometry.

Table 2 - Details of Small-Scale Sequential Separation of U, Pu, Am

Step	Volume	Details
Eichrom UTEVA Resin	0.5 ml	100-150 μm
Clean resin	3 x 2 ml 1 M HCl	
Condition resin	2 ml 3 M HNO_3	
Condition resin	1 ml 7.2 M HNO_3 -0.3% H_2O_2	
Dissolve sample and load	0.5 ml 7.2 M HNO_3 -0.3% H_2O_2	Elute Am
Wash	0.5 ml 7.2 M HNO_3 -0.3% H_2O_2	Elute Am
Wash	2 ml 7.2 M HNO_3 -0.3% H_2O_2	Elute Am
Wash	1 ml 9 M HCl	Elute Pu
Wash	2 x 2 ml 5 M HCl-0.5 M oxalic acid	Elute Pu
Final wash	2 x 2 ml 1 M HCl	Elute U

Mass Spectrometry Methods

After purification and resuspension, samples were analyzed using a Thermo Neptune Plus MC-ICP-MS. Isotopes were collected in static mode for each element with the full mass range of interest collected simultaneously, with the exception of samples traced with ^{244}Pu , which were collected using a peak-hopping analyses method due to the lack of certified Pu standards containing ^{244}Pu for the bias correction calculations. Samples were analyzed using an enhanced ionization setup consisting of a Cetac Aridus II desolvating nebulizer with jet-sampler and x-skimmer cones following a previously published procedure.⁴⁶

Alpha Spectrometry Methods

Americium samples were traced with ^{243}Am , purified as described above, and final purified samples were electroplated onto stainless steel disks and measured by alpha spectrometry. Alpha spectra were recorded using an Ortec Ensemble 8-channel alpha spectrometer equipped with a 19 keV FWHM 300 mm^2 Si-detector. The ^{241}Am content of the sample was quantified from the original tracer activity and the measured $^{241}\text{Am}/^{243}\text{Am}$ activity ratio in the alpha spectrum.

Results and discussion

Chemical purification details

One of the principal goals of this study was to develop isotope dilution methods for the analysis of large particles of nuclear fuel. Isotope dilution is considered a primary measurement method by international metrological groups, and provides highly accurate isotopic and inter-elemental ratios.⁴⁷ However, isotope dilution mass spectrometry analysis of actinides typically employs chemical purification of the elements of interest to eliminate potential interferences from both isobaric elements (e.g. ^{241}Am interference on ^{241}Pu) and polyatomic species (e.g. $^{238}\text{UH}^+$ interference on ^{239}Pu). A major challenge in the chemical purification of very small actinide samples is the potential introduction of background during the purification process.^{33, 48} This impact can be quantified by running the purification process with no added analyte (the process blank). For this work, a scaled-down purification method was developed that minimizes the introduction of uranium into the sample. A typical process blank for the procedure was on the order of ~ 1 pg ^{238}U , as compared to 10-50 pg for more standard procedures in our laboratory. The procedure uses extraction chromatography to separate U, Pu, and Am from a single fraction, conserving sample and maximizing detection limits for low-level samples. The Pu and Am fractions from the first column were further purified using established ion exchange techniques for ultra-trace samples.⁴⁴⁻⁴⁵

The details of the FIB particle analysis depended on the relative actinide concentrations in the cube. For FIB cubes with relatively higher actinide concentrations (ca. 8 or more ng total U), the sample was split in half. One half of the sample was traced with ^{242}Pu , ^{233}U , and ^{243}Am and purified for U, Pu, and Am. The other half of the sample was left untraced and purified for additional isotopic measurements. For FIB cubes with lower actinide contents, the samples were treated as a single aliquot, traced with ^{244}Pu , ^{233}U , ^{243}Am , purified, and analyzed by mass spectrometry.

Mass Spectrometry Results

The Neptune Plus used for analyses in this study is equipped with an array of Faraday and ion counting detectors specifically configured and optimized for actinide analyses.⁴⁶ This configuration allows for the simultaneous collection of all isotopes of the elements of interest at a wide range of concentrations, while also monitoring for potential interferences. Mass and detector biases were calculated using a sample-standard bracketing technique with appropriate, well-

calibrated standards for each element. With each set of analyses, matrix-matched and isotopically appropriate QC standards were included and treated as unknowns. All QC standards were within uncertainty of their respective certificate values confirming the accuracy of the technique.

Previous studies have described techniques for removing, or mathematically accounting for, interfering species in ultra-trace analyses of actinides through combinations of background measurements, increased mass resolution, and reaction chamber MS/MS techniques.⁴⁹⁻⁵⁰ Due to the small sizes of the samples in this study, these techniques were not applicable; however, recognizing the importance of ensuring interference free measurements, detailed mass scans were taken of all samples prior to data acquisition to confirm adequate chemical purification had occurred.

The multi-ion-counting and enhanced ionization techniques developed for this study allow for the measurement of sub-picogram, and in one case sub-femtogram, quantities of Pu isotopes while maintaining the accuracy and precision necessary for investigating the isotopic variability present in the reactor. These are among the smallest aliquots of Pu measured by ICP-MS, and represent a significant advancement in measurement capabilities for ultra-trace actinides, particularly in association with corresponding U and Am analyses.

Fuel samples and isotopic results

To evaluate the ability of our new methods to quantify spatial variations in isotopic composition in the reactor fuel, large particle samples were obtained at different axial and radial locations in an archived spent fuel rod (I-334) from the Belgian BR3 PWR reactor. The samples were cut as cubes of dimensions $10 \times 10 \times 10$ μm or $20 \times 20 \times 20$ μm using a FIB.

The samples were obtained from 4 different locations along the length of the fuel rod. A schematic of the sampling is shown in Figure 1. The fuel rod was 1 meter in length, and samples were taken at positions 1, 2, 3, and 4, which were 0.05, 0.22, 0.51, and 0.98 meters from the top of the fuel rod, respectively. Position 3 is near the center of the rod, and positions 1 and 4 are near the ends of the fuel rod. Figure 1 shows the sampling locations overlaid with a gross gamma scan along the axis of the fuel rod which was taken inside the hot cell at INL. The gross gamma activity is highest near the center of the fuel rod, indicating a higher degree of burnup in this region.

The FIB samples were also taken from several different radial locations. The fuel rod has a radius of 3900 μm , and FIB particles were cut at locations near the center, near the edge or rim, and at intermediate positions of the fuel rod (Figure 2). Table 1 provides a list of sample IDs and locations; the first number of the sample ID corresponds to the axial sampling location, while the letters represent different radial positions. Table 3 shows the measured U content for each of the samples. Samples containing less than 1ng U likely represent cases where the FIB particle may have partially broken during handling and transportation (see Supporting Information). It is worth noting that despite the fact that much of the sample may have been lost, in some cases where a "complete" sample was measured next to a "partial" sample (e.g., 1-C3 and 1-C4), the isotopic and

1 intra-element values are consistent between the two samples.
2 This demonstrates the strength of this technique across a range
3 of sample concentrations, yielding consistent and accurate
4 results even when only a small fraction of the material
5 remained.
6

7 **Isotopic composition as a function of axial position**

8 The actinide isotopic analyses indicate major differences in the
9 extent of burnup that depend on the axial position in the fuel
10 rod. The differences in burnup revealed by the actinide analyses
11 mirror the gross gamma spectrum of the fuel rod (Figure 3),
12 with central position 3 showing a much higher burnup than the
13 terminal positions 1 and 4, and position 2 at an intermediate
14 level. The difference in burnup is perhaps most evident in the
15 $^{240}\text{Pu}/^{239}\text{Pu}$ ratio, which is considerably higher in position 3C
16 (0.329(1)) than either position 2C (0.145(4)) or position 4C
17 (0.131(1)). The trend is also evidenced in $^{235}\text{U}/^{238}\text{U}$ ratios which
18 decrease as the amount of burnup increases from position 1C
19 (0.0663(2)) to 2C (0.04530(3)) to the center 3C (0.0407(1)).

20 Figures 4 and 5 show plots of the uranium isotope ratios
21 overlaid with the gross gamma scan. The results of the uranium,
22 plutonium, and americium analyses are shown in Tables 3, 4,
23 and 5 respectively. Inter-element actinide ratios, another
24 indicator of degree of burnup, are shown in Table 6.
25
26
27
28
29
30
31
32
33
34
35
36
37
38
39
40
41
42
43
44
45
46
47
48
49
50
51
52
53
54
55
56
57
58
59
60

Table 3 - Uranium measurements of large particle samples cut from the BR3 fuel rod I-334

Sample ID	Axial Sampling position	Radial location (μm from edge)	^{238}U (ng per sample)	$^{234}\text{U}/^{238}\text{U}$	$^{235}\text{U}/^{238}\text{U}$	$^{236}\text{U}/^{238}\text{U}$
1-A1*	1	200	13.2(1)	0.000436(2)	0.05456(25)	0.00546(3)
1-A2	1	200	16.20(2)	0.000546(1)	0.06385(6)	0.00567(3)
1-B	1	400	17.23(2)	0.000541(1)	0.06556(8)	0.00578(3)
1-C1*	1	3000	0.138(6)	0.000443(80)	0.0543(4)	0.00417(35)
1-C2	1	3000	0.227(2)	0.000564(17)	0.06622(36)	0.00483(6)
1-C3	1	3000	147(4)	0.000564(3)	0.06630(23)	0.00517(3)
1-C4	1	3000	0.895(3)	0.000553(4)	0.06656(21)	0.00514(2)
2-A	2	5	10.31(2)	0.000553(2)	0.03949(3)	0.01038(1)
2-B	2	40	9.28(2)	0.000514(2)	0.03823(3)	0.00990(1)
2-C	2	1781	10.57(2)	0.000490(2)	0.04530(3)	0.00880(1)
3-A	3	36	11.00(2)	0.000522(1)	0.03255(10)	0.01146(6)
3-B*	3	101	0.135(1)	0.000461(6)	0.02811(10)	0.00916(4)
3-C	3	3755	10.03(1)	0.000498(1)	0.04073(11)	0.00980(7)
4-A1	4	190	15.22(11)	0.000541(4)	0.06534(32)	0.00555(3)
4-A2	4	190	0.797(3)	0.000557(4)	0.06314(25)	0.00537(2)
4-B	4	900	18.25(2)	0.000554(1)	0.06715(6)	0.00535(4)
4-C1	4	3003	11.59(7)	0.000523(4)	0.06818(34)	0.00473(3)
4-C2	4	3173	170.3(6)	0.000550(4)	0.06884(34)	0.00470(3)
4-C3	4	3173	129.4(2)	0.000566(1)	0.06939(4)	0.00475(2)

*The samples 1-A1, 1-C1, and 3-B have isotopic compositions outside that expected for these types of samples, and two of which are the smallest samples analyzed during this project. It is likely that given the small amount of U in these samples, that they represent mixing between the sample and natural uranium introduced from the copper and aluminum sample holder. In the case of positions 1-A1 and 1-C1, duplicate FIB samples (with much higher sample sizes) demonstrate that these small samples do indeed represent mixed analyses. Sample 1-A1, while having a total U content similar to many others in this study, has an isotopic composition inconsistent with other adjacent (1-A2) and nearby (1-B) samples and likely represents a sample contaminated with natural uranium.

Table 4 - Plutonium measurements of large particle samples cut from the BR3 fuel rod I-334

Sample ID	Axial sampling position	Radial location (μm from edge)	^{239}Pu (μg per sample)	$^{240}\text{Pu}/^{239}\text{Pu}$	$^{241}\text{Pu}/^{239}\text{Pu}^*$	$^{242}\text{Pu}/^{239}\text{Pu}$	$^{238}\text{Pu}/^{239}\text{Pu}^*$
1-A1	1	200	51.9(19)	0.1594(58)	0.0104(12)	0.0048(9)	
1-A2	1	200	59.6(31)	0.1586(7)	0.0088(3)	0.0053(2)	
1-B	1	400	55.6(32)	0.1572(8)	0.0085(3)	0.0052(2)	
1-C1	1	3000	0.40(6)	0.1447(82)	0.0084(14)	0.0048(14)	
1-C2	1	3000	0.75(3)	0.137(12)	0.0071(29)	0.0049(26)	
1-C3	1	3000	462(13)	0.1447(36)	0.0085(7)	0.0036(4)	0.00402(4)
1-C4	1	3000	2.90(4)	0.1451(27)	0.0089(7)	0.0037(3)	
2-A	2	5	289(11)	0.2999(56)	0.0325(20)	0.0446(13)	
2-B	2	40	173(4)	0.3029(36)	0.0319(4)	0.0431(6)	
2-C	2	1781	64.7(27)	0.2775(49)	0.0231(11)	0.0252(9)	
3-A	3	36	158.8(35)	0.3536(13)	0.0351(13)	0.0716(7)	
3-B	3	101	1.06(2)	0.3492(49)	0.0396(17)	0.0656(25)	
3-C	3	3755	44.1(10)	0.3289(13)	0.0239(9)	0.0369(5)	
4-A1	4	190	75.7(19)	0.1535(40)	0.0095(3)	0.0043(2)	
4-A2	4	190	7.24(9)	0.1540(23)	0.0101(4)	0.0045(3)	
4-B	4	900	62.0(36)	0.1464(7)	0.0076(3)	0.0041(2)	
4-C1	4	3003	33.1(7)	0.1335(35)	0.0074(3)	0.0028(2)	
4-C2	4	3173	446(7)	0.1312(29)	0.0073(2)	0.0027(1)	0.0034(1)
4-C3	4	3173	383(25)	0.1308(5)	0.0063(2)	0.0029(1)	

*Measurement reference date: 9/2/2016

Table 5 - Americium measurements of large particle samples cut from the BR3 fuel rod I-334 and ^{241}Pu - ^{241}Am chronometer model age values

Sample ID	Axial sampling position	Radial location (μm from edge)	^{241}Am (pg per sample)	$^{243}\text{Am}/^{241}\text{Am}$	^{241}Pu — ^{241}Am model age (years)*
1-A1	1	200	2.44(4)		35.8(24)
1-A2	1	200	3.21(5)		42.0(9)
1-B	1	400	2.82(5)		41.5(9)
1-C1	1	3000	0.014(2)		34.2(46)
1-C2	1	3000	0.026(2)		37.3(88)
1-C3	1	3000	18.3(3)	0.0040(1)	36.5(18)
1-C4	1	3000	0.146(2)		40.9(17)
2-A	2	5	32.2(3)	0.0287(2)	33.2(14)
2-B	2	40	18.8(2)	0.0284(2)	33.1(5)
2-C	2	1781	5.38(6)	0.0212(4)	34.0(11)
3-A	3	36	28.7(4)		38.8(9)
3-B	3	101	0.206(3)		38.3(10)
3-C	3	3755	6.02(9)		40.7(9)
4-A1	4	190	3.25(7)		36.0(8)
4-A2	4	190	0.49(1)		44.2(9)
4-B	4	900	2.48(4)		39.3(10)
4-C1	4	3003	1.16(3)		36.9(11)
4-C2	4	3173	14.9(3)	0.0031(1)	36.2(8)
4-C3	4	3173	12.8(2)		39.3(10)

*Age reference date: 9/2/2016

Table 6 - Measured actinide ratios of large particle samples cut from the BR3 fuel rod I-334

Sample ID	Axial sampling position	Radial location (μm from edge)	total Pu: total U	total Am: total Pu
1-A1	1	200	0.0043(2)	0.040(2)
1-A2	1	200	0.004(2)	0.046(3)
1-B	1	400	0.0035(2)	0.043(3)
1-C1	1	3000	0.0019(3)	0.030(6)
1-C2	1	3000	0.0059(3)	0.030(2)
1-C3	1	3000	0.0034(1)	0.034(1)
1-C4	1	3000	0.00349(5)	0.043(1)
2-A	2	5	0.037(1)	0.082(3)
2-B	2	40	0.0244(6)	0.080(2)
2-C	2	1781	0.0077(3)	0.064(3)
3-A	3	36	0.0201(4)	0.123(3)
3-B	3	101	0.011(2)	0.133(3)
3-C	3	3755	0.0058(1)	0.098(3)
4-A1	4	190	0.0054(1)	0.037(1)
4-A2	4	190	0.0099(1)	0.058(1)
4-B	4	900	0.0037(2)	0.034(2)
4-C1	4	3003	0.003(1)	0.030(1)
4-C2	4	3173	0.00278(4)	0.029(1)
4-C3	4	3173	0.0031(2)	0.029(2)

Rim effect

Reactor models predict a sharp increase in the extent of burnup approaching the rim of a fuel rod due to greater neutron moderation in this area.^{13, 16-18} However, there is a limited amount of experimental analytical data with fine spatial resolution near the edges fuel pellets.¹⁴ The methods developed as part of this work can measure actinide isotopic and inter-element ratios with micron-level resolution, providing a window into the rim effect in the spent BR3 fuel rod I-334.

The BR3 particle samples clearly demonstrate the rim effect. Uranium, plutonium, and americium analyses reveal significant increases in burnup near the rim of the rod across all axial positions. For example, in axial position 3 the measured $^{240}\text{Pu}/^{239}\text{Pu}$ ratio increased from 0.329(1) at the center to 0.354(1) at a position 36 μm from the edge (Figure 6). Likewise, the $^{235}\text{U}/^{238}\text{U}$ ratio decreased from 0.0407(1) at the center to 0.0326(1) at 36 μm from the edge due to fission and neutron capture reactions of ^{235}U . Also for axial position 3, the actinide inter-element Pu:U ratio increased upon moving from the center to the rim (Figure 6). Figure 7 shows related trends in $^{240}\text{Pu}/^{239}\text{Pu}$ and Pu:U ratios as a function of distance from the edge for axial position 4; all four axial positions exhibit similar isotopic trends arising from the rim effect.

When all sampled positions are considered, all metrics are consistent with variable burnup both axially and radially. Figure 8 shows a three isotope plot of $^{235}\text{U}/^{238}\text{U}$ versus $^{236}\text{U}/^{238}\text{U}$; the measured ratios for the FIB particle samples fall on a line. This consistent trend in the uranium isotopic ratios reveals that as the burnup in the reactor fuel increases, the $^{235}\text{U}/^{238}\text{U}$ ratio decreases and the $^{236}\text{U}/^{238}\text{U}$ ratio increases. The $^{240}\text{Pu}/^{239}\text{Pu}$ ratio for each sample is shown in color scale and parallels the

trends observed for the uranium isotope ratios, with higher $^{240}\text{Pu}/^{239}\text{Pu}$ ratios accompanying samples with higher $^{236}\text{U}/^{238}\text{U}$ and lower $^{235}\text{U}/^{238}\text{U}$ ratios.

Consistent trends are also observed for the $^{240}\text{Pu}/^{239}\text{Pu}$, $^{241}\text{Pu}/^{239}\text{Pu}$, and $^{242}\text{Pu}/^{239}\text{Pu}$ atom ratios. Figure 9 shows a three isotope plot of $^{240}\text{Pu}/^{239}\text{Pu}$ versus $^{241}\text{Pu}/^{239}\text{Pu}$; the trend shows that the observed $^{241}\text{Pu}/^{239}\text{Pu}$ ratio increases with increasing $^{240}\text{Pu}/^{239}\text{Pu}$. The minor isotope ^{242}Pu mirrors this trend, with the measured $^{242}\text{Pu}/^{239}\text{Pu}$ ratio increasing as the degree of burnup in the fuel increases. The $^{242}\text{Pu}/^{239}\text{Pu}$ ratio is shown in color scale in Figure 9 and correlates strongly with the $^{240}\text{Pu}/^{239}\text{Pu}$ and $^{241}\text{Pu}/^{239}\text{Pu}$ ratios.

The observed isotopic and inter-element trends in reactor burnup are entirely consistent with those expected as a function of position in the fuel rod. However, such complete isotopic information is rarely derived from the analysis of particle samples. This work highlights the potential to gain detailed isotopic information by applying isotope dilution mass spectrometry techniques to large single particle samples.

Americium chronometry

A significant advantage of the methods developed in this work is that by using isotope dilution and chemical purification, ^{241}Am and ^{241}Pu can be quantified in particle samples. ^{241}Am is chemically separated from its isobar ^{241}Pu and measurements of both analytes can be used to calculate the age of the samples, which reflects the cooling time of the reactor fuel.³¹⁻³² The ages of Pu particles have previously been described using SIMS⁵¹ and ICP-MS,⁵² however those studies made use of the Pu-U chronometers and/or focused on analyses of standards which are expected to yield less complicated separation and analysis conditions than spent fuel. Additionally, in previous studies Pu was a major component rather than at trace levels in a larger matrix.

The analysis of the BR3 FIB samples demonstrates that accurate ages can be obtained for single particle samples of complicated chemical composition. Using measured ^{241}Pu and ^{241}Am values, model ages for the BR3 FIB particles were calculated as shown in equation 1 and Table 5.

$$(1) \quad t = \frac{\ln \left[1 - \frac{N_2^t}{N_1^t} \left(\frac{\lambda_2 - \lambda_1}{\lambda_1} \right) \right]}{\lambda_1 - \lambda_2}$$

where $N_1 = ^{241}\text{Pu}$ and $N_2 = ^{241}\text{Am}$.

The average age for the nineteen FIB samples was 37.8(3.1) years, corresponding to a date of 11/14/1978 (Figure 10). This calculated age is entirely consistent with the known period of operation for cores 4A and 4B of the BR3 reactor. Both cores had rod I-334 in them, and operated from 7/15/1976 to 4/15/1978 and from 6/22/1979 to 9/26/1980, respectively. Because ^{241}Pu decays with a relatively short half-life (14.3 years), and the reactor was operated for multiple years, the age calculated for the samples represents a convolution of time since the first irradiation and time since the last irradiation

(cooling time). It is thus expected that the calculated age dates back to roughly an average of the operating lifespan of this rod.

Conclusions

This paper describes the development and application of scaled-down methods for the analysis of single particles of nuclear fuel using chemical purification and isotope dilution mass spectrometry. Nineteen individual particles cut from a spent fuel rod from the Belgian BR3 reactor were analyzed for U, Pu, and Am isotopic compositions and inter-element ratios. The isotope dilution techniques are able to accurately resolve differences in axial and radial burnup in the spent fuel rod. In addition, ^{241}Pu - ^{241}Am chronometry performed on the particles generated model ages that were consistent with the known operating history of the BR3 reactor. This represents the first time that the ^{241}Pu - ^{241}Am chronometer has been applied to "real-world" single particle samples.

Studies in recent years have made use of FIB cut samples of nuclear fuel for investigating fine-scale microstructures and isotopic heterogeneity of fuel starting material.⁵³⁻⁵⁶ However, the techniques used in these studies do not provide high-precision inter- or intra-element ratios needed to calculate precise ages or detailed reactor histories.

Spatially controlled samples of spent nuclear reactor fuel provide the opportunity to investigate the heterogeneity of burnup and reaction throughout the operation of a reactor. The level of information provided from this type of analysis will allow for a higher understanding and increased fidelity in reactor model simulations as results like this are incorporated into multi-dimensional reactor simulations. Future studies incorporating the high-precision isotopic and quantitative elemental ratio techniques described here, along with high-fidelity reactor modeling will yield invaluable information for nuclear safeguards and materials understanding.

Author Contributions

Both authors contributed equally to all aspects of the study.

Conflicts of interest

There are no conflicts to declare.

Acknowledgements

The authors thank multiple colleagues at Idaho National Laboratory for their expertise and support: Katelyn Wachs and Kevin Carney provided the axial gamma scan of the fuel rod; Brian Frickey and Paul Lind cut the fuel and prepared sample mounts; Dean Blanton and Brandon Miller cut the FIB cubes, took SEM photographs, and shipped the samples. We also thank Nicholas Luciano and Andrew Conant for discussions on an early draft of this paper. We would also like to thank Travis Tenner for helpful discussions and SEM images of related samples.

This work was funded by the National Nuclear Security Administration's Office of Defence Nuclear Nonproliferation Research and Development. Los Alamos National Laboratory is operated by Triad National Security, LLC, for the National Nuclear Security Administration of U.S. Department of Energy (Contract No. 89233218CNA000001).

Notes and references

1. Boulyga, S.; Konegger-Kappel, S.; Richter, S.; Sangély, L., Mass spectrometric analysis for nuclear safeguards. *Journal of Analytical Atomic Spectrometry* **2015**, *30* (7), 1469-1489.
2. Kraiem, M.; Richter, S.; Kuhn, H.; Stefaniak, E. A.; Kerckhove, G.; Truyens, J.; Aregbe, Y., Investigation of uranium isotopic signatures in real-life particles from a nuclear facility by thermal ionization mass spectrometry. *Anal Chem* **2011**, *83* (8), 3011-6.
3. Tandon, L.; Hastings, E.; Banar, J.; Barnes, J.; Beddingfield, D.; Decker, D.; Dyke, J.; Farr, D.; FitzPatrick, J.; Gallimore, D.; Garner, S.; Gritz, R.; Hahn, T.; Havrilla, G.; Johnson, B.; Kuhn, K.; LaMont, S.; Langner, D.; Lewis, C.; Majidi, V.; Martinez, P.; McCabe, R.; Mecklenburg, S.; Mercer, D.; Meyers, S.; Montoya, V.; Patterson, B.; Pereyra, R. A.; Porterfield, D.; Poths, J.; Rademacher, D.; Ruggiero, C.; Schwartz, D.; Scott, M.; Spencer, K.; Steiner, R.; Villarreal, R.; Volz, H.; Walker, L.; Wong, A.; Worley, C., Nuclear, chemical, and physical characterization of nuclear materials. *Journal of Radioanalytical and Nuclear Chemistry* **2008**, *276* (2), 467-473.
4. Taylor, T. B., Nuclear Safeguards. *Annu. Rev. Nucl. Sci.* **1975**, *25*, 407-421.
5. *Safeguards Implementation Practices Guide on Establishing and Maintaining State Safeguards Infrastructure*; IAEA: Vienna, Austria, 2018.
6. *International Safeguards in the Design of Reprocessing Plants*; Vienna, Austria, 2019; No. NF-T-3.2 p. 1-76.
7. Boulyga, S.; Becker, J. S., Determination of Uranium Isotopic Composition and ^{236}U Content of Soil Samples and Hot Particles Using Inductively Coupled Plasma Mass Spectrometry. *Fresenius J. Anal. Chem.* **2001**, *370*, 612-617.
8. Wolf, S. F.; Bowers, D. L.; Cunnane, J. C., Analysis of High Burnup Spent Nuclear Fuel by ICP-MS. *Journal of Radioanalytical and Nuclear Chemistry* **2005**, *263*, 581-586.
9. Lisman, F. L.; Maeck, W. J.; Rein, J. E., Determination of Nuclear Fuel Burnup from Fission Product Analysis. *Nuclear Science and Engineering* **2017**, *42* (2), 215-219.
10. Robel, M.; Isselhardt, B.; Ramon, E.; Hayes, A.; Gaffney, A.; Borg, L.; Lindvall, R.; Erickson, A.; Carney, K.; Battisti, T.; Conant, A.; Ade, B.; Trelue, H.; Weber, C., A composite position independent monitor of reactor fuel irradiation using Pu, Cs, and Ba isotope ratios. *J Environ Radioact* **2018**, *195*, 9-19.
11. Conant, A.; Erickson, A.; Robel, M.; Isselhardt, B., Sensitivity and Uncertainty Analysis of Plutonium and Cesium Isotopes in Modeling of BR3 Reactor Spent Fuel. *Nuclear Technology* **2017**, *197* (1), 12-19.
12. Dobrin, R. I.; Craciunescu, T.; Pavelescu, M., CANDU and TRIGA Fuel Burn-up Determination Using Axial and Tomographic Gamma-Scanning. *Romanian Reports in Physics* **2011**, *63* (4), 1009-1017.
13. Neuber, J. C. In *Evaluation of Axial and Horizontal Burnup Profiles*, Technical Committee Meeting on Implementation of Burnup Credit in Spent Fuel Management Systems, Vienna, Austria, Agency, I. A. E., Ed. ISSN 1011-4289: Vienna, Austria, 2000; pp 183-211.
14. Lassmann, K.; O'Carroll, C.; van de Laar, J.; Walker, C. T., The Radial Distribution of Plutonium in High Burnup UO_2 Fuels. *Journal of Nuclear Materials* **1994**, *208*, 223-231.
15. Soba, A.; Lemes, M.; González, M. E.; Denis, A.; Romero, L., Simulation of the behaviour of nuclear fuel under high burnup conditions. *Annals of Nuclear Energy* **2014**, *70*, 147-156.
16. Matzke, H. J., Radiation Damage in Nuclear Fuel Materials: The "Rim" Effect in UO_2 and Damage in Inert Matrices for Transmutation of Actinides. *Nuclear Instruments and Methods in Physics Research B* **1996**, *116*, 121-125.
17. Barani, T.; Pizzocri, D.; Cappia, F.; Luzzi, L.; Pastore, G.; Van Uffelen, P., Modeling high burnup structure in oxide fuels for application to fuel performance codes. part I: High burnup structure formation. *Journal of Nuclear Materials* **2020**, *539*.
18. Trelue, H. R.; Fensin, M. L.; Elson, J. S.; Galloway, J. D.; Adigun, B. J. *Simulated Irradiated Nuclear Fuel Isotopic Compositions*; Los Alamos National Laboratory: 2016; LA-UR-16-22945.
19. Noirot, J.; Desgranges, L.; Lamontagne, J., Detailed characterisations of high burn-up structures in oxide fuels. *Journal of Nuclear Materials* **2008**, *372* (2-3), 318-339.
20. Rondinella, V. V.; Wiss, T., The high burn-up structure in nuclear fuel. *Materials Today* **2010**, *13* (12), 24-32.
21. Williamson, T. L.; DeVore, M. A.; Tenner, T. J.; Smith, R.; Inabinet, L.; Mershon, J.; Hiller, J.; Wellons, M. S., Towards the Synthesis of Mixed Actinide Particulate Reference Materials: Microscopy and Spectroscopic Characterization of U/Ce-containing Specimens. *Microscopy and Microanalysis* **2019**, *25* (S2), 1548-1549.
22. Boulyga, S.; Prohaska, T., Determining the Isotopic Compositions of Uranium and Fission Products in Radioactive Environmental Microsamples Using Laser Ablation ICP-MS with Multiple Ion Counters. *Anal. Bioanal. Chem* **2008**, *390*, 531-539.
23. Kappel, S.; Boulyga, S.; Dorta, L.; Gunther, D.; Hattendorf, B.; Koffler, D.; Laaha, G.; Leisch, F.; Prohaska, T., Evaluation Strategies for Isotope Ratio Measurements of Single Particles by LA-MC-ICPMS. *Anal. Bioanal. Chem* **2013**, *405*, 2943-2955.
24. Yongyang, S.; Wei, W.; Zhiming, L.; Hu, D.; Guoqing, Z.; Jiang, X.; Xiangjun, R., Direct detection and isotope analysis of individual particles in suspension by single particle mode MC-ICP-MS for nuclear safety. *Journal of Analytical Atomic Spectrometry* **2015**, *30* (5), 1184-1190.
25. Callis, E. L.; Abernathy, R. M., High-Precision Isotope Analyses of Uranium and Plutonium by Total Sample Volatilization and Signal Integration. *International Journal of Mass Spectrometry and Ion Processes* **1991**, *103*, 93-105.
26. Kraiem, M.; Richter, S.; Kuhn, H.; Aregbe, Y., Development of an improved method to perform single particle analysis by TIMS for nuclear safeguards. *Anal Chim Acta* **2011**, *688* (1), 1-7.
27. Lee, C. G.; Iguchi, K.; Inagawa, J.; Suzuki, D.; Esaka, F.; Magara, M.; Sakurai, S.; Watanabe, K.; Usuda, S., Development in fission track-thermal ionization mass spectrometry for particle analysis of safeguards environmental samples. *Journal of Radioanalytical and Nuclear Chemistry* **2007**, *272* (2), 299-302.
28. Chen, Y.; Shen, Y.; Chang, Z.-Y.; Zhao, Y.-G.; Guo, S.-L.; Cui, J.-Y.; Liu, Y., Studies on analyzing single uranium-bearing particle by FT-TIMS. *Radiation Measurements* **2013**, *50*, 43-45.
29. Heumann, K., Isotope Dilution Mass Spectrometry. *International Journal of Mass Spectrometry and Ion Processes* **1992**, *118-119*, 575-592.
30. Heumann, K., Isotope Dilution Mass Spectrometry (IDMS) of the Elements. *Mass Spectrometry Reviews* **1992**, *11*, 41-67.
31. Byerly, B. L.; Stanley, F.; Spencer, K.; Colletti, L.; Garduno, K.; Kuhn, K.; Lujan, E.; Martinez, A.; Porterfield, D.; Rim, J.; Schappert, M.; Thomas, M.; Townsend, L.; Xu, N.; Tandon, L., Forensic

- 1 investigation of plutonium metal: a case study of CRM 126. *Journal*
2 *of Radioanalytical and Nuclear Chemistry* **2016**, *310* (2), 623-632.
- 3 32. Fitzgerald, R.; Inn, K. G. W.; Horgan, C., How old is it?—
4 ²⁴¹Pu/²⁴¹Am nuclear forensic chronology reference materials.
5 *Journal of Radioanalytical and Nuclear Chemistry* **2015**, *307* (3),
6 2521-2528.
- 7 33. Boulyga, S. F.; Koepf, A.; Konegger-Kappel, S.; Macsik, Z.;
8 Stadelmann, G., Uranium isotope analysis by MC-ICP-MS in sub-ng
9 sized samples. *Journal of Analytical Atomic Spectrometry* **2016**, *31*
10 (11), 2272-2284.
- 11 34. Esaka, F.; Suzuki, D.; Miyamoto, Y.; Magara, M., Determination
12 of plutonium isotope ratios in individual uranium-plutonium mixed
13 particles with inductively coupled plasma mass spectrometry.
14 *Journal of Radioanalytical and Nuclear Chemistry* **2015**, *306* (2),
15 393-399.
- 16 35. Kraiem, M.; Richter, S.; Erdmann, N.; Kuhn, H.; Hedberg, M.;
17 Aregbe, Y., Characterizing uranium oxide reference particles for
18 isotopic abundances and uranium mass by single particle isotope
19 dilution mass spectrometry. *Anal Chim Acta* **2012**, *748*, 37-44.
- 20 36. Shinonaga, T.; Esaka, F.; Magara, M.; Klose, D.; Donohue, D.,
21 Isotopic analysis of single uranium and plutonium particles by
22 chemical treatment and mass spectrometry. *Spectrochimica Acta*
23 *Part B: Atomic Spectroscopy* **2008**, *63* (11), 1324-1328.
- 24 37. Salbu, B., Actinides associated with particles. In *Radioactivity in*
25 *the Environment*, Kudo, A., Ed. Elsevier: 2001; Vol. 1, pp 121-138.
- 26 38. Ketterer, M. E.; Szechenyi, S. C., Determination of plutonium
27 and other transuranic elements by inductively coupled plasma mass
28 spectrometry: A historical perspective and new frontiers in the
29 environmental sciences. *Spectrochimica Acta Part B: Atomic*
30 *Spectroscopy* **2008**, *63* (7), 719-737.
- 31 39. Walther, C.; Denecke, M. A., Actinide Colloids and Particles of
32 Environmental Concern. *Chemical Reviews* **2013**, *113* (2), 995-1015.
- 33 40. Taylor, R. N.; Warneke, T.; Milton, J. A.; Croudace, I. W.;
34 Warwick, P. E.; Nesbitt, R. W., Plutonium isotope ratio analysis at
35 femtogram to nanogram levels by multicollector ICP-MS. *Journal of*
36 *Analytical Atomic Spectrometry* **2001**, *16* (3), 279-284.
- 37 41. Quinto, F.; Hrncsek, E.; Krachler, M.; Shotyk, W.; Steier, P.;
38 Winkler, S. R., Determination of (²³⁹Pu, ²⁴⁰Pu, ²⁴¹Pu and
39 ²⁴²Pu) at femtogram and attogram levels - evidence for the
40 migration of fallout plutonium in an ombrotrophic peat bog profile.
41 *Environ Sci Process Impacts* **2013**, *15* (4), 839-47.
- 42 42. Aitkaliyeva, A.; Madden, J. W.; Miller, B. D.; Cole, J. I.,
43 Implementation of focused ion beam (FIB) system in
44 characterization of nuclear fuels and materials. *Micron* **2014**, *67*,
45 65-73.
- 46 43. Hou, X.; Zhang, W.; Wang, Y., Determination of Femtogram-
47 Level Plutonium Isotopes in Environmental and Forensic Samples
48 with High-Level Uranium Using Chemical Separation and ICP-
49 MS/MS Measurement. *Anal Chem* **2019**, *91* (18), 11553-11561.
- 50 44. Knab, D., Determination of Americium in Small Environmental
51 Samples. *Anal. Chem.* **1979**, *51*, 1095-1097.
- 52 45. Oldham, W. J.; Matteson, B. S.; Miller, J. L.; Lake, C. T.; Attrep,
53 M., Rusty nails adsorb trace plutonium from the environment.
54 *Journal of Radioanalytical and Nuclear Chemistry* **2012**, *296* (2),
55 889-892.
- 56 46. Pollington, A. D.; Kinman, W. S.; Hanson, S. K.; Steiner, R. E.,
57 Polyatomic interferences on high precision uranium isotope ratio
58 measurements by MC-ICP-MS: applications to environmental
59 sampling for nuclear safeguards. *Journal of Radioanalytical and*
60 *Nuclear Chemistry* **2015**, *307* (3), 2109-2115.
47. Richter, W., Primary Methods of Measurement in Chemical
Analysis. *Accred Qual Assur* **1997**, *2*, 354-359.
48. Esaka, F.; Suzuki, D.; Magara, M., Identifying uranium particles
using fission tracks and microsampling individual particles for
analysis using thermal ionization mass spectrometry. *Anal Chem*
2015, *87* (5), 3107-13.
49. Pointurier, F.; Hémet, P.; Hubert, A., Assessment of plutonium
measurement in the femtogram range by ICP-MS; correction from
interfering polyatomic species. *J. Anal. At. Spectrom.* **2008**, *23* (1),
94-102.
50. Pointurier, F.; Pottin, A.-C.; Hémet, P.; Hubert, A., Combined use
of medium mass resolution and desolvation introduction system for
accurate plutonium determination in the femtogram range by
inductively coupled plasma-sector-field mass spectrometry.
Spectrochimica Acta Part B: Atomic Spectroscopy **2011**, *66* (3-4),
261-267.
51. Wallenius, M.; Tamborini, G.; Koch, L., The "Age" of Plutonium
Particles. *Radiochim. Acta* **2001**, *89*, 55-58.
52. Miyamoto, Y.; Suzuki, D.; Esaka, F.; Magara, M., Accurate
purification age determination of individual uranium-plutonium
mixed particles. *Anal Bioanal Chem* **2015**, *407* (23), 7165-73.
53. Kautz, E.; Burkes, D.; Joshi, V.; Lavender, C.; Devaraj, A.,
Nanoscale Spatially Resolved Mapping of Uranium Enrichment. *Sci*
Rep **2019**, *9* (1), 12302.
54. Kautz, E.; Cliff, J.; Lach, T.; Reilly, D.; Devaraj, A., Correlating
nanoscale secondary ion mass spectrometry and atom probe
tomography analysis of uranium enrichment in metallic nuclear
fuel. *Analyst* **2021**, *146* (1), 69-74.
55. Bachhav, M.; Gan, J.; Keiser, D.; Giglio, J.; Jädnäs, D.;
Leenaers, A.; Van den Berghe, S., A novel approach to determine
the local burnup in irradiated fuels using Atom Probe Tomography
(APT). *Journal of Nuclear Materials* **2020**, 528.
56. Reilly, D. D.; Beck, C. L.; Buck, E. C.; Cliff, J. B.; Duffin, A. M.;
Lach, T. G.; Liezers, M.; Springer, K. W.; Tedrow, S. J.; Zimmer, M.
M., Focused ion beam for improved spatially-resolved mass
spectrometry and analysis of radioactive materials for uranium
isotopic analysis. *Talanta* **2020**, *211*, 120720.

Figures

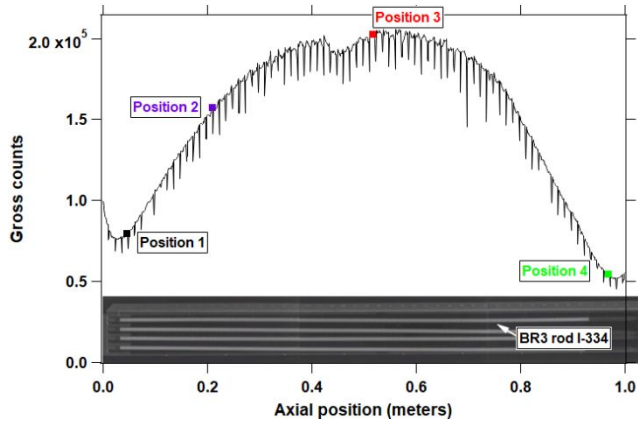
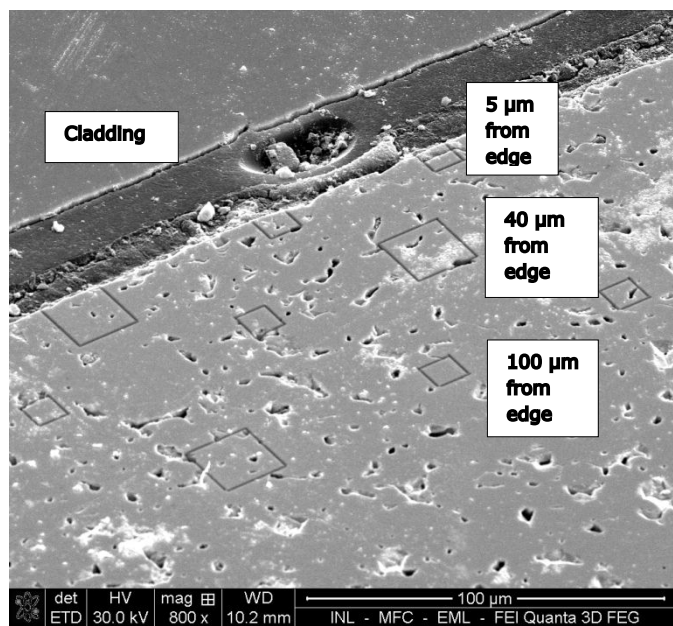


Figure 1 - Gross gamma scan of fuel rod I-334 from the BR3 reactor. The axial sampling positions 1, 2, 3, and 4 are superimposed on the scan. Sharp negative peaks in the gamma scan indicate small gaps between individual fuel pellets within the overall rod. An autoradiograph image of fuel rod I-334 is shown at the bottom of the plot.



23 Figure 2 - SEM image of FIB fuel particle cutting near the rim of the BR3 fuel rod at axial
24 position 2. Large and small squares are the initial outlines of multiple 20 x 20 μm
25 and 10 x 10 μm cubes respectively. There is a small band of dark epoxy between the
26 cladding and the fuel; this was added during sample processing.

27
28
29
30
31
32
33
34
35
36
37
38
39
40
41
42
43
44
45
46
47
48
49
50
51
52
53
54
55
56
57
58
59
60

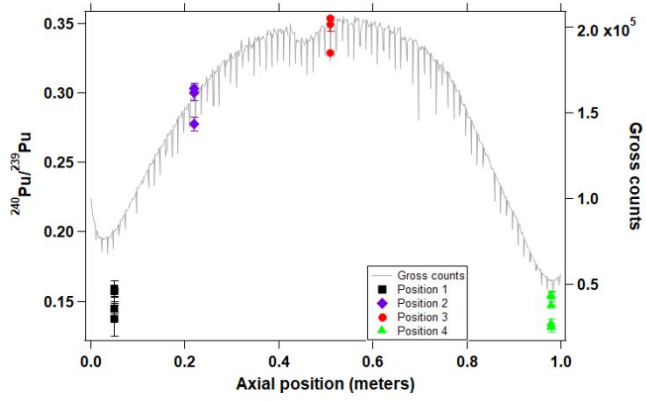


Figure 3 - Measured $^{240}\text{Pu}/^{239}\text{Pu}$ ratios at the different axial sampling positions in the fuel rod I-334.

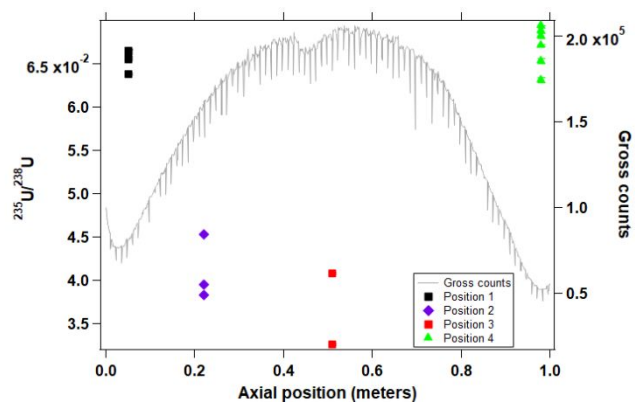


Figure 4 - Measured $^{235}\text{U}/^{238}\text{U}$ ratios at the different axial sampling positions in the fuel rod I-334.

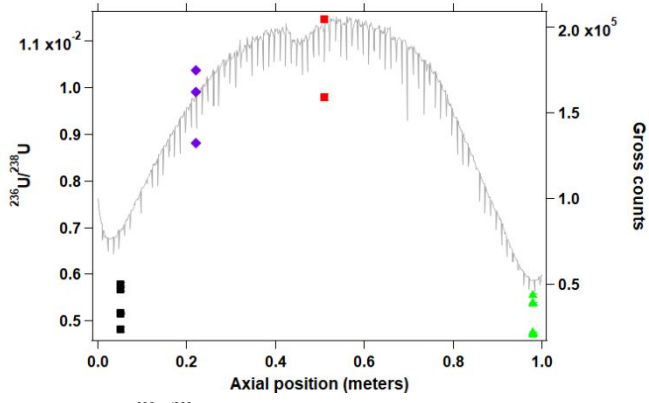


Figure 5 - Measured $^{236}\text{U}/^{238}\text{U}$ ratios at the different axial sampling positions in the fuel rod I-334.

1
2
3
4
5
6
7
8
9
10
11
12
13
14
15
16
17
18
19
20
21
22
23
24
25
26
27
28
29
30
31
32
33
34
35
36
37
38
39
40
41
42
43
44
45
46
47
48
49
50
51
52
53
54
55
56
57
58
59
60

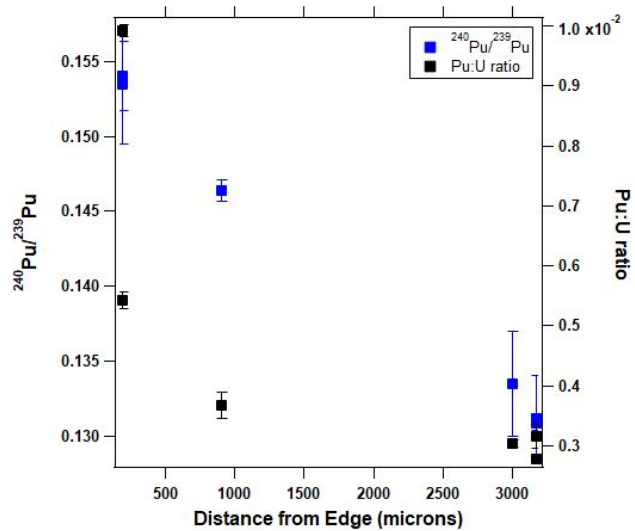


Figure 6 - For axial sampling position 3 (0.51 m from the top of the fuel rod), a plot of $^{240}\text{Pu}/^{239}\text{Pu}$ and Pu:U ratios as a function of radial distance.

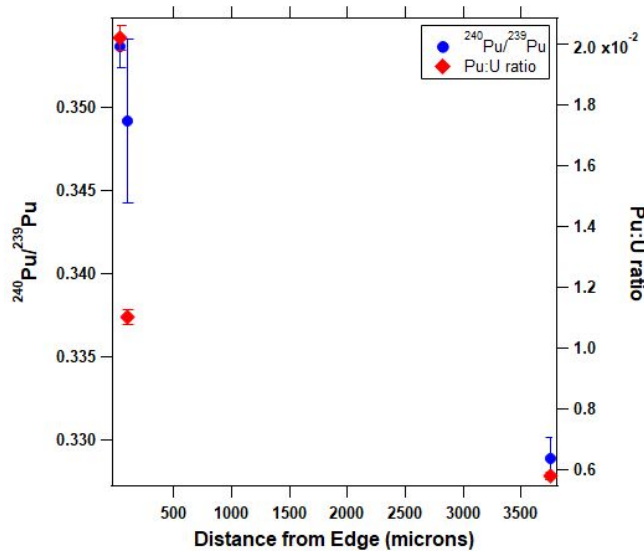


Figure 7 - For axial sampling position 4 (0.98 m from the top of the fuel rod), a plot of $^{240}\text{Pu}/^{239}\text{Pu}$ and Pu:U ratios as a function of radial distance.

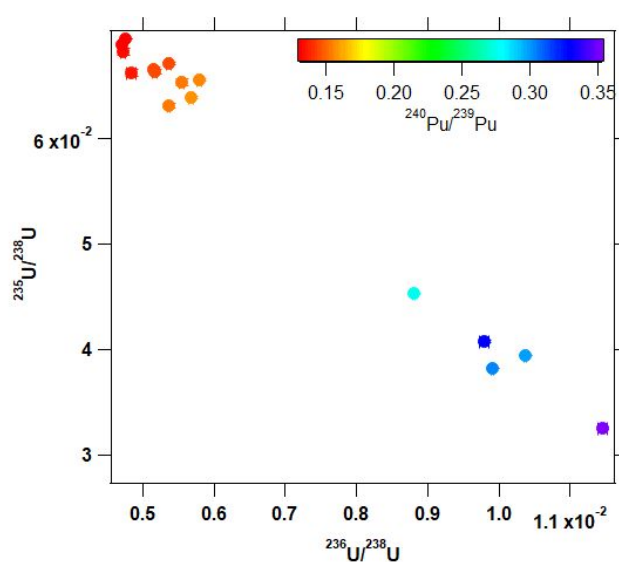


Figure 8 - Three isotope plot of $^{235}\text{U}/^{238}\text{U}$ versus $^{236}\text{U}/^{238}\text{U}$ for all samples. The measured $^{240}\text{Pu}/^{239}\text{Pu}$ ratio is shown in color scale.

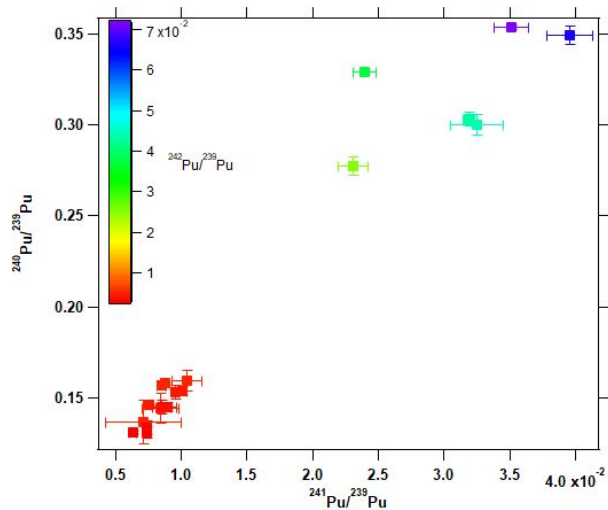


Figure 9 - Three isotope plot of $^{240}\text{Pu}/^{239}\text{Pu}$ versus $^{241}\text{Pu}/^{239}\text{Pu}$ for all samples. The measured $^{242}\text{Pu}/^{239}\text{Pu}$ ratio is shown in color scale.

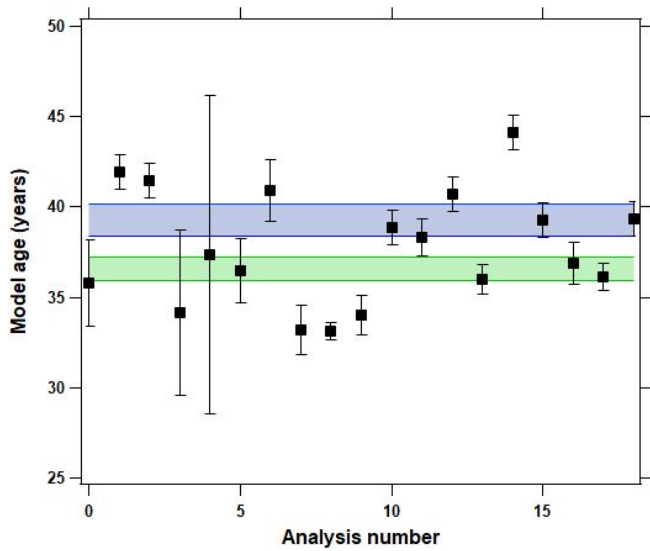


Figure 10 - Model ages for the BR3 fuel particle samples, calculated from the ^{241}Pu - ^{241}Am chronometer. Shaded bands represent the periods when this fuel rod was operating in the reactor (July 1976-April 1978 and June 1979-September 1980), demonstrating good agreement between calculated ages and known operating history.